WaveComBE

mmWave Communications in the Built Environments

WaveComBE_D2.2

Report on estimated channel parameters in the built environment

Version v1.0 Date: 2021/08/30

Document properties:

Grant Number:	766231
Document Number:	D2.2
Document Title:	Report on estimated channel parameters in the built environment
Partners involved:	Durham University
Authors:	Amar Al-jzari, Monika Drozdowska, and Sana Salous
Contractual Date of Delivery:	2021/09/30
Dissemination level:	CO[1]
Version:	1.0
File Name:	WaveComBE D2.2_v1.0

[1] CO = Confidential, only members of the consortium (including the Commission Services)

PU = Public

1 Table of contents

2 Executive Summary

This document describes wideband single-input single-output (SISO) and single-input multiple-output (SIMO) indoor directional channel measurements collected on the Durham University Campus. SISO and SIMO measurements were conducted in the 60 GHz ISM band in a meeting room, a classroom, a seminar room, an office room, and a computer laboratory. The indoor directional measurements were performed using the rotated directional antenna (RDA) based method. This document also presents human blockage (HB) measurements at the 60 GHz band in a seldom reported environment, a corridor style set up with computers (computer clusters). The present measurements were carried out using the Multi-band Frequency Modulated Continuous Wave (FMCW) channel sounder developed at Durham University. Moreover, based on the measurements in the meeting room the simulations in ray tracing (RT) simulator developed at Universitat Politècnica de València (UPV) were performed.

The main goal of this document is to present different statistical channel parameters, such as power delay profile (PDP), power angle profile (PAP), root mean square delay spread (RMS DS), angular spread (AS), and path loss (PL). These parameters were measured and estimated for different possible antenna orientations, which include line of sight (LoS), obstructed line of sight (OLoS), and non-line of sight (NLoS). The impact of polarization on the channel parameters, the delay spread model as well as the angular spread model as a function of the size of the environment are thoroughly studied. For the meeting room scenario RMS DS and PL were simulated using RT. The impact of the environment size and Tx-Rx distance on mentioned channel parameters were studied. Furthermore, human blockage attenuations (HBS) are investigated, and different blockage models such as Kirchhoff knife-edge diffraction (KED) model, METIS (mobile and wireless communications enablers for the twenty-twenty information society) KED model, and geometrical theory of diffraction (GTD) are used to simulate the effect of human body shadowing.

3 List of figures

4 List of tables

5 List of Acronyms and Abbreviations

5G	Fifth generation
ADC	Analog-to-digital converter
AoA	Angle of arrival
AoD	Angle of departure
AS	Angular spread
BS	Boresight
CDF	Cumulative distribution function
FMCW	Frequency Modulated Continuous Wave
GTD	Geometrical theory of diffraction
ITU	International Telecommunication Union
KED	Kirchhoff knife-edge diffraction
HB	Human blockage
HBS	Human blockage shadwoing
LoS	Line of sight
MPCs	Multi-path components
METIS	Mobile and wireless communications enablers for the twenty-twenty information society
NBS	Non-boresight
NLoS	Non-line of sight
OLoS	Obstructed line of sight
PAP	Power angle profile
PDP	Power delay profile
PL	Path loss
RMS DS	Root Mean Square Delay Spread
Rx	Receiver
SIMO	Single-input multiple-output
SISO	Single-input single-output
Tx	Transmitter

1. Introduction

The demand for higher data traffic in wireless communication networks and the congestion of the spectrum below 6 GHz has encouraged the wireless industry, research community, and regulators to consider alternative bands. The millimeter wave (mm-Wave) frequency band has been identified for next 5G wireless networks due to the availability of large contiguous bandwidths that can be exploited to achieve a high data rate, with 5-7 GHz being available around the 60 GHz band. However, these frequency bands suffer from many challenges due to the very small wavelengths, resulting in different channel propagation characteristics compared with traditional WLAN systems operating at lower frequency bands [1-2]. Thus, various indoor propagation measurements and models are needed in these frequency bands for future networks system design [3]. In [1]-[10], channel measurements were conducted at different frequency bands, such as 15, 28, 45, 60, and 73 GHz bands. The measured scenarios include office rooms, corridors, hallways, museum, shopping mall, and conference room to estimate path loss, delay spread, small-scale spatial and temporal statistics, and wall and floor penetration loss. Most of the abovementioned measurements were performed with a single antenna at both the Tx and Rx sides, using different channel sounders in various scenarios which could have a significant impact on the channel properties. Therefore, SISO and SIMO indoor measurements in multi-scenarios using the same channel sounder are scarce and critical for providing a good comparison of the propagation channel characteristics and an identical channel model framework at these mm-Wave bands.

In [11]-[15], human blockage measurements and modeling have been performed at different mm-Wave bands. Most of the human blockage measurements were conducted in a small office room. Hence, it is very important to perform human blockage measurements in a real indoor scenario to assess the impact of human body shadowing on the 5G communications systems. To the best of the author's knowledge, so far, no measurements have been reported for a corridor style with computer clusters on human blockage.

In this document, wideband SISO, SIMO and human blockage measurements were conducted at the frequency band (59.6-65.6 GHz) within typical indoor environments to measure and estimate different statistical channel parameters as well as human blockage loss. Based on one of measured scenarios the simulations with RT method were performed. The propagation channel characteristics for different angular orientations and the human body shadowing attenuation are obtained at these mm-Wave bands. The polarization effects on the channel parameters, the human blockage models, as well as the delay spread model and the angular spread model as a function of the room size are thoroughly studied. Section 2 outlines the channel parameters to be estimated. Section 3 and 4 covers the associated SISO and SIMO measurement results, analysis, and modeling, respectively. Section 5 describes the associated human blockage measurement results, analysis, and modeling. Section 6 presents the simulations methodology and results, and some guidelines regarding saving environmental data for planned simulations. Concluding remarks are given in Section 7.

2. Estimated Channel Parameters

The measured Power Delay Profile (PDP), expressed in (1), is used to estimate different relative channel parameters.

$$PDP = P(\tau) = \frac{1}{M}\sum_{m=1}^{M}|h_m(t_m,\tau)|^2 \quad (1)$$

where M is the total number of channel impulse responses captured at each angular rotation, and τ is the time delay.

The RMS Delay Spread (RMS DS) is an essential channel parameter to illustrate the time dispersion properties of the channel due to multipath. The RMS DS is the square root of the second central moment of the PDP and can be calculated as:

$$\tau_{rms} = RMS\ DS = \sqrt{\frac{\sum_{n=1}^{N} P_n\ {\tau_n}^2}{\sum_{n=1}^{N} P_n} - (\frac{\sum_{n=1}^{N} P_n\ \tau_n}{\sum_{n=1}^{N} P_n})^2} \quad (2)$$

where τ_n and P_n are the delay and the power of the nth path.

The Angular Spread (AS) is an important channel parameter to characterize the dispersion properties of the Power Angle Profile (PAP). The AS is related to the directivity of the MPCs and can be calculated as:

$$\emptyset_m = \arg(\frac{\sum_{k=1}^{K} P_R(\emptyset_k)\ e^{i\emptyset_k}}{\sum_{k=1}^{K} P_R(\emptyset_k)}) \quad (3)$$

$$\emptyset_{AS} = AS\ = \sqrt{\frac{\sum_{k=1}^{K} P_R(\emptyset_k)\ ((\emptyset_k-\emptyset_m)^2)}{\sum_{k=1}^{K} P_R(\emptyset_k)}}\ , \quad (4)$$

$$PAP = P_R(\emptyset_k)\ = \sum_{n=1}^{N} P(\tau_n,\emptyset_k) \quad (5)$$

where $\emptyset_m$ is the mean azimuthal angle of arrival or departure, K is the number of each angle position and $P_R(\emptyset_k)$ is the PAP (received power at each azimuth angle $\emptyset_k$) which is in the range of +/- π.

Path Loss (PL) is an essential channel parameter for estimating the link budget and coverage in the design of wireless networks. PL represents the ratio between the transmitted power and the received power without the overall system and antenna gains. PL can be expressed as:

$$PL\ [dB] = -P_{RX} + G_{RX} + G_{TX} - P_{TX} - L_{Sy} \quad (6)$$

$$P_{RX} = \sum_{n=1}^{N} P_n \quad (7)$$

where P_{TX} is the transmitted power in (dBm), P_{RX} is the received power in (dBm), (G_{TX} & G_{RX}) are the Tx and Rx antenna gains in (dBi), respectively, and L_{Sy} is the overall system loss in dB.

3. SISO Angle of Arrival Measurements

3.1 Measurements Methodology

SISO AoA measurements were conducted using a custom-designed multi-band chirp (FMCW) channel sounder [8] in a seminar room and a computer laboratory environment, shown in Fig. 1. Both environments are set up with multiple chairs, desks, and tables and are equipped with a large projection screen and whiteboard. The present measurements were performed with a 6 GHz bandwidth in the frequency range of (59.6 - 65.6 GHz) with a waveform repetition frequency of 1.22 kHz. A Flann MD249-AA omni-directional antenna was used at the transmitter (Tx), while at the receiver (Rx), a horn antenna with 20 dBi gain and 18° beamwidth was used to estimate different relative channel parameters. The measurements were conducted for both line of sight (LoS), and non-line of sight (NLoS), scenarios with the Tx location fixed at one end of the room while the Rx was moved onto predefined locations within the scenario as shown in Fig. 2. The arrow at the Rx position represents the main beam's direction at a rotation angle of zero degrees. The Tx antenna height was set at 2.3-2.6 m which is close to the typical height of an access point, while the Rx antenna was set at 1.5 m for a typical user. To investigate the wideband channel in the angular domain and to synthesize an omni-directional received signal, a CCTV positioner is used to rotate the directional antennas in steps of 15° to cover the full 360° in azimuth. Hence, for measuring AoA, the Tx unit was fixed while the Rx was rotated in the azimuth plane to cover the full rotation. At each angular rotation, the data were recorded for one second duration with a 40 MHz sampling rate ADC.

(a) Seminar room.

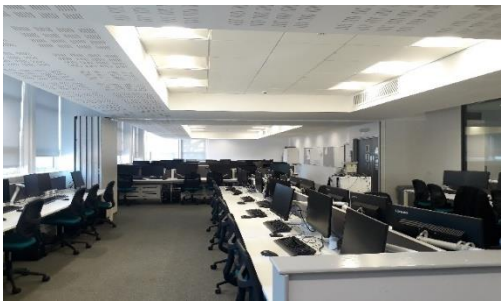

(b) Computer Lab.

Fig. 1: Photos of different measurement environments.

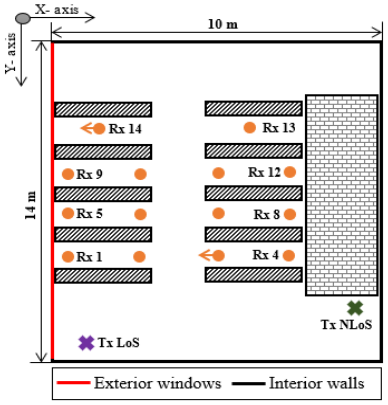

(c) Seminar room.

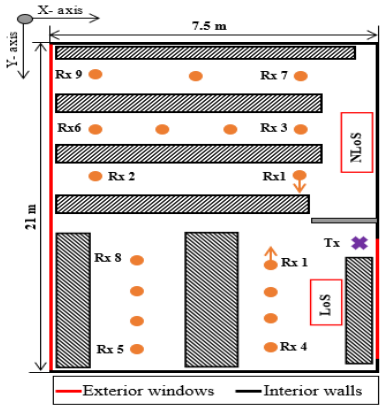

(d) Computer Lab.

Fig. 2: Layout of different measurement environments.

3.2 Results and analyses

- **Power Delay Profile (PDP):**

The data were processed with 2 GHz bandwidth to obtain the PDP, which was then used to estimate different relative channel parameters. Fig. 3 displays the measured angular PDPs versus the Rx rotation angle of one LoS location and one NLoS location in the seminar room environment, where the LoS location exhibited a strong component in the boresight angle (-90°) at around 10 ns with few multipath components, while in the NLoS case, more MPCs can be observed due to the reflections from the glass windows and concrete walls, which result in larger delay spread. The impact of beam alignment can be further seen in Fig. 4, which represents the directional measured PDPs at different azimuth angles in one of the measured locations. A strong component is detected when the receiver antenna was pointing towards the transmitter and when it was facing away from it, the power is gradually reduced.

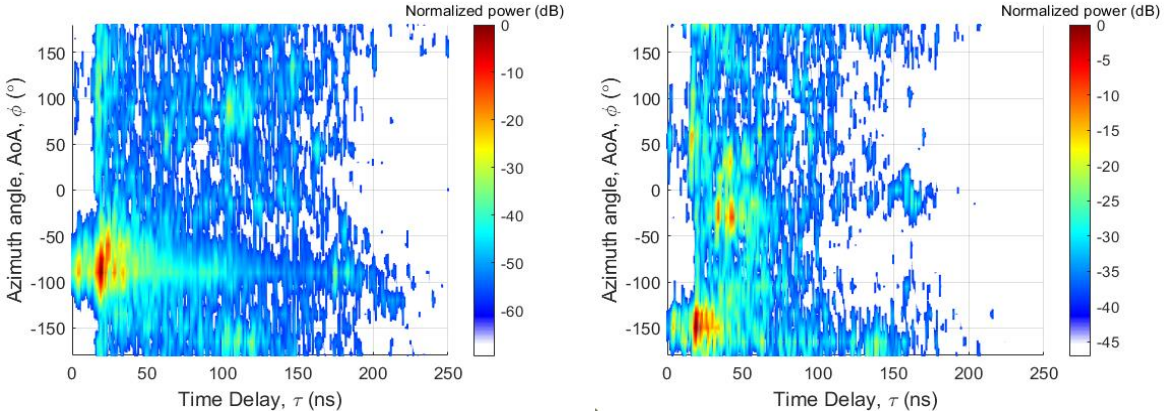

(a) LoS scenario. (b) NLoS scenario.

Fig. 3: Relative PDP vs. Rx rotation angle in a seminar room environment.

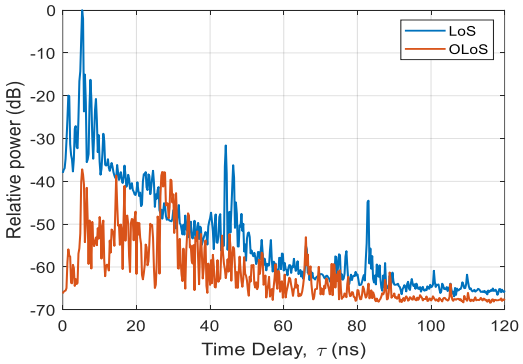

Fig. 4: Directional PDPs at different azimuth angle for LoS scenario in a seminar room environment.

- **Power Angle Profile (PAP):**

The directional received power at each azimuthal angle for LoS location and NLoS location in the seminar room environment is shown in Fig. 5. In the LoS location, it can be seen that the main

received power corresponding to the LoS path is achieved when the Tx and Rx antennas are pointing towards each other, while the reflected components from different angles occurr when the Rx antenna is oriented to the opposite direction of the Tx antenna. In the NLoS location, it can be identified that the received power is concentrated at different directions due to the large number of reflections that result in more multipath components in the azimuth domain compared with the LoS location.

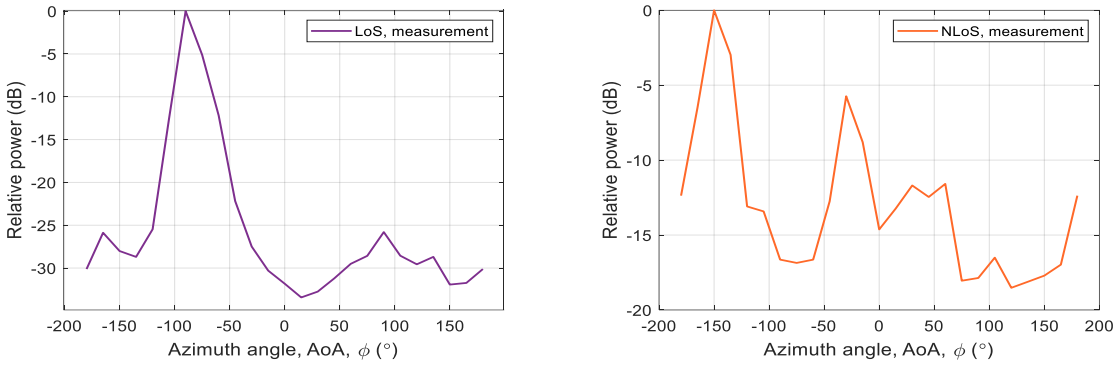

(a) LoS location. (b) NLoS location.

Fig. 5: Power angle profile in a seminar room environment.

- **Root Mean Square Delay Spread (RMS DS)**

The RMS delay spread was estimated with a 20 dB threshold from the peak power in each PDP. Fig. 6 displays the CDFs of the RMS delay spread for the seminar room and computer laboratory environment where the estimated delay spread was classified based on the angular direction between the Tx and Rx antennas, as LoS when the receive antenna was pointing towards the transmitter, OLoS when the receive antenna was physically in the LoS of the transmitter but the antenna beam is misaligned with the transmitter antenna, and NLoS when the receiver and transmitter were obstructed by a partition, as shown in Fig. 2. Fig. 6 shows the increase in the RMS delay spread of the OLoS and NLoS scenarios due to the misalignment of the beam and the presence of the partition. To characterize the delay spread, the CDFs were fitted with a Gaussian normal distribution N (μ, σ) and the estimated parameter of the distribution (σ) as well as the 10%, 50% and 90% values of the CDF are given in Table 1.

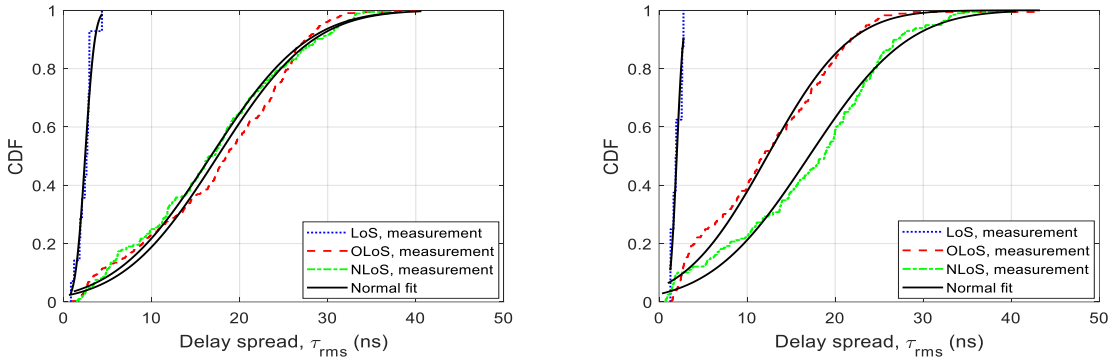

(a) Seminar room. (b) Computer Lab.

Fig. 6: CDF of RMS DS for different measured environments.

Table 1: RMS DS statistics in (ns) for different measured environment.

Type of Env.	**RMS Delay Spread Statistics CDF=10%; CDF=50%; CFD=90%; and σ fitting parameter**		
	LoS (BS)	OLoS (NBS)	NLoS
Seminar room	0.98; 2.60; 2.94; 0.86	3.91; 18.50; 27.48; 8.51	4.78; 18.16; 31.13; 8.65
Computer Lab.	1.29; 1.88; 2.65; 0.59	2.61; 11.76; 21.74; 7.43	3.36; 18.79; 26.69; 8.81

- **Angular Spread (AS)**

The angular spread is used to characterize the dispersion properties of the PAP where the PAP is the received power at each azimuth angle. Fig. 7 shows the computed CDF of the AS values for the seminar room and computer lab. environment in the LoS and NLoS scenarios. Table 2 gives a summary of the AS values in degrees at CDF levels of 10%, 50%, and 90% as well as the corresponding standard deviation ($\sigma_{\phi_{AS}}$) in the LoS and NLoS scenarios for each measured environment. The results indicate the LoS locations exhibit on average a smaller AS compared with NLoS locations due to less reflectors and scatterers. This is also because the relative power in the LoS component is much stronger than the reflected components in the NLoS case. Similar results were reported at 6-60 GHz in indoor scenarios [16]. The angular spread results emphasize the fact that indoor environments are multipath rich and, therefore, high angular spread values are achieved.

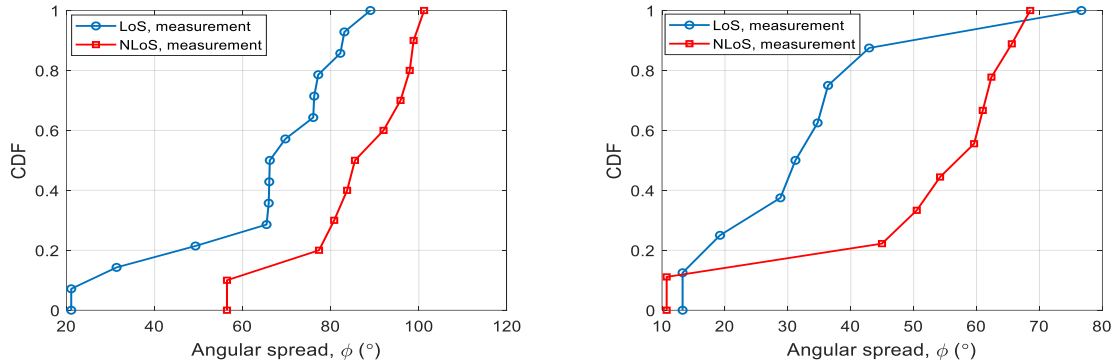

(a) Seminar room. (b) Computer lab.

Fig. 7: CDF of AS for different measured environments.

Table 2: AS statistics in degrees (°) for different measured environment.

Type of Env.	**Angular Spread Statistics CDF=10%; CDF=50%; CFD=90%; and $\sigma_{\phi_{AS}}$**	
	LoS scenario	NLoS scenario
Seminar room	25.19; 66.17; 82.73; 19.46	56.44; 85.51; 98.82; 13.51
Computer Lab.	13.27; 31.20; 49.67; 19.17	10.73; 56.90; 65.89; 17.51

- **Directional and Synthesized Omni-directional Path Loss (PL)**

Path loss model parameters were investigated using the floating Intercept (FI) model. The FI model parameters, including the distance coefficient (α) and the PL intercept coefficient (PL_o) were estimated from the present measurements. A detailed calculation of the FI model can be found in [9]. In the present work, the PL was estimated for different possible antenna alignments with significant differences ranging 10 to more than 30 dB. Fig. 8 (a)-(c) presents measured PL data for the LoS peak (strongest component), the OLoS (synthesized back beam) and the NLoS (strongest component) cases, as well as the corresponding model fits. To compare the directional with a synthesized omni-directional receive antenna, the PL for the LoS and NLoS scenarios was synthesized from the directional measurements as shown in Fig. 9. Table 3 provides a summary of the PL modelling results for the directional and synthesized omni-directional PL in both measured environments. It can be seen that the synthesized omni-directional beam results are close to the strongest component results. This is due to the fact that the received power was dominated by the LoS path. This table also indicates that the PL intercept is higher for the synthesized back beam compared with the strongest component and synthesized omni-directional. Furthermore, higher synthesized omni-directional PL intercept was observed in the NLoS case compared with the LoS case due to the obstruction between the Tx and the Rx antennas.

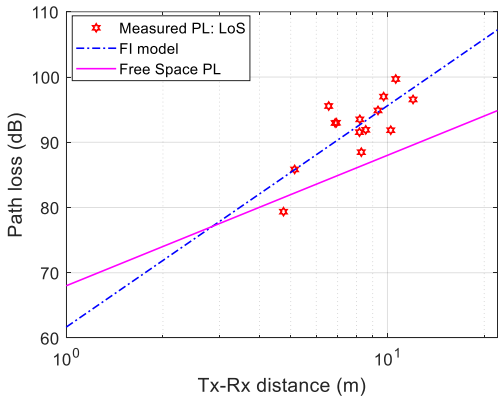

(a) LoS Peak (Strongest Component) Scenario.

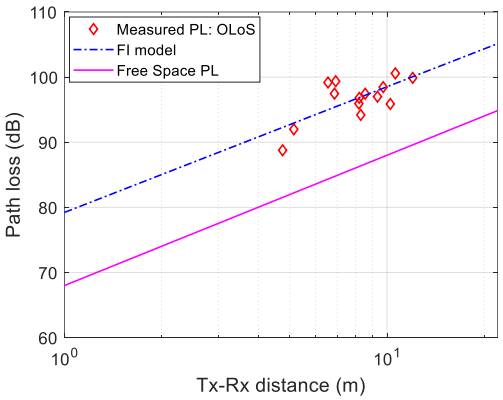

(b) OLoS Angles (Synthesized back beam) Scenario.

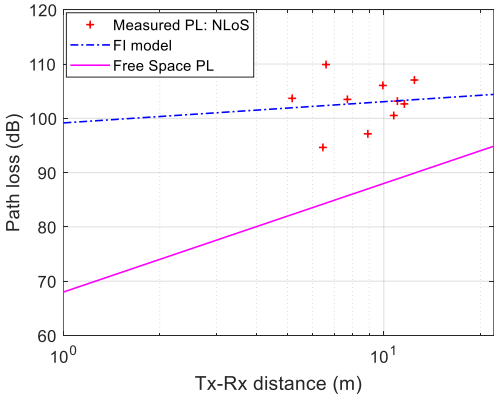

(c) NLoS (Strongest Component) Scenario.

Fig. 8: PL for different receive angles in a seminar room environment.

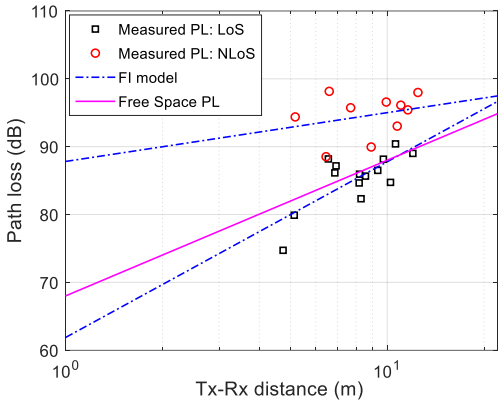

Fig. 9: Synthesized Omni-directional PL in a seminar room environment.

Table 3: PL model parameters of the FI model for a seminar room and a computer lab environment.

Type of Env.	Scenario	PL estimation method	FI model (α, β, σ)
Seminar room	LoS	Strongest beam	61.7, 3.4, 3.1
		Synthesized back beam	79.2, 1.9, 2.2
		Synthesized omni-directional	61.9, 2.6, 2.6
	NLoS	Strongest beam	99.1, 0.4, 4.3
		Synthesized omni-directional	87.8, 0.7, 2.9
Computer Lab.	LoS	Strongest beam	64.4, 3.3, 1.9
		Synthesized back beam	75.1, 2.6, 1.3
		Synthesized omni-directional	61.1, 2.8, 1.1
	NLoS	Strongest beam	97.3, 0.4, 3.3
		Synthesized omni-directional	86.2, 1.3, 2.1

4. SIMO Angle of Arrival Measurements

4.1 Measurements Methodology

SIMO dual-polarized channel measurements with 1 x 2 antenna configurations were conducted using Durham University's FMCW channel sounder [8] in a meeting room, an office room, and a computer laboratory environment, shown in Fig. 10. The measured environments are set up with multiple chairs, desks, tables, and computers. The measurements were performed with a 6 GHz bandwidth in the 60 GHz ISM band with a waveform repetition frequency of 1.22 kHz. An omni-directional antenna was used at the Tx, while at the Rx, two horn antennas with different polarization (V-H) were used to investigate the impact of polarization on the propagation channel characteristics. The measurements were conducted in a LoS scenario with the Tx location fixed at one end of the room while the Rx was moved onto predefined locations within the scenario as shown in Fig. 11. The arrow at the Rx position represents the main beam's direction at a rotation angle of zero degrees. The Tx antenna height was set at 2.4-2.6 m which is close to the typical height of an access point, while the Rx antenna was set at 1.6 m for a typical user. To investigate the wideband channel in the angular domain, a CCTV rotator is used to steer the directional antennas in steps of 10° to cover the full rotation in azimuth plane. Therefore, 36 data files were recorded at each location, corresponding to the full 360° azimuthal coverage. At each angular rotation, the data were recorded for one second with a 40 MHz sampling rate ADC. Table 4 gives a summary of the channel measurement set-up parameters for each measured environment.

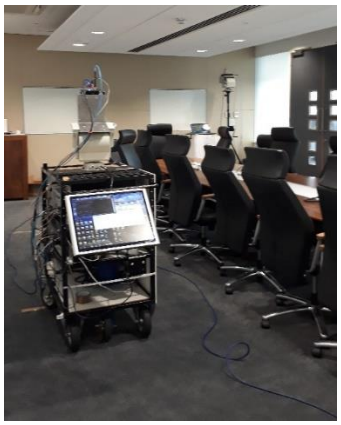

(a) Meeting room.

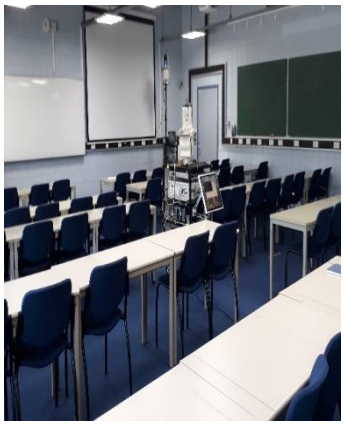

(b) Office room.

(c) Computer lab.

Fig. 10: Photos of different measurement environments.

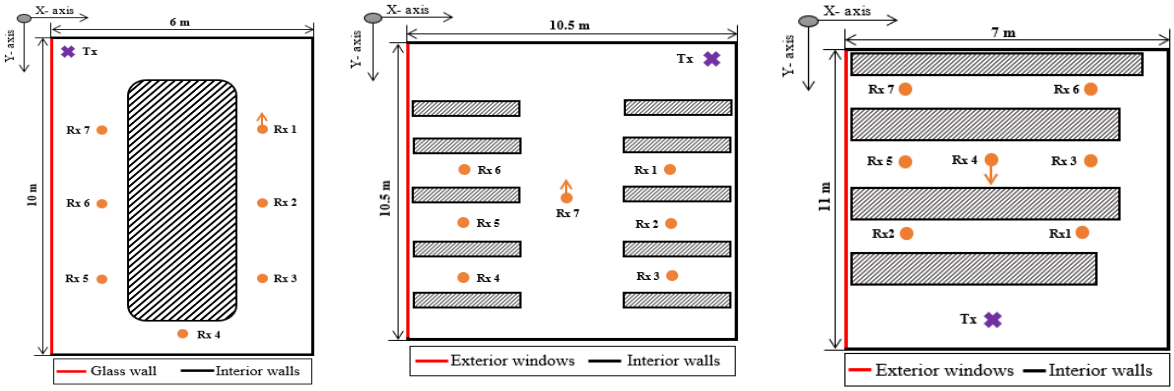

(a) Meeting room. (b) Office room. (c) Computer lab.

Fig. 11: Layout of different measurement environments.

Table 4: Channel measurements set-up parameters.

Frequency range	**59.6 – 65.6 GHz**
RF bandwidth	6 GHz
Analysis bandwidth	2 GHz
Sampling rate	40 MHz
Sweep rate	1.22 kHz
Antenna Configuration	1 x 2 (SIMO)
Tx/Rx polarization	VV & VH
Tx Antenna type	Omni-directional antenna
Rx Antenna type	Horn antenna (20 dBi gain, 18° HPBW)
Tx antenna height	2.4-2.6 m
Rx antenna height	1.6 m

4.2 Results and analyses

- **Power Delay Profile (PDP):**

The data were analyzed to obtain the PDP of each angle for the co-polar link and the cross-polar link to investigate the impact of both co-polarized and cross-polarized antenna configurations on different relevant channel parameters. Fig. 12 presents an example of the PDP at one location in the office room environment as a function of the Rx rotation angle for different polarizations (V-V & V-H). The strong component can be observed at around 40° on the co-polar link (V-V) which corresponds to the boresight angle when the Tx and Rx antennas are pointing to each other. Other peaks appear at around 150° and -60° which corresponds to the non-boresight angles when the Rx antenna is orientated to the opposite direction. In general, the co-polarized channels have higher received signal levels than the cross-polarized channels, as shown in Fig. 12, this is due to the polarization mismatch of the Tx and Rx antennas. In comparison to co-polarized antennas, cross-

polarized antennas have a greater delay spread due to the presence of more MPCs as a result of the large number of reflections within the environment.

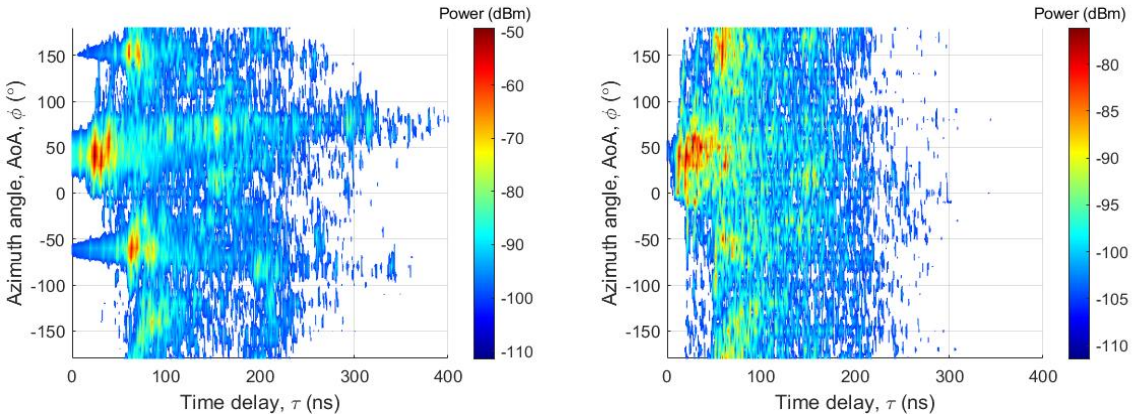

(a) Co-polarized configuration. (b) Cross-polarized configuration.

Fig. 12: PDP vs. Rx rotation angle in an office room environment.

- **Root Mean Square Delay Spread (RMS DS)**

Fig. 13 displays the CDF of the RMS DS values for an office room environment. During the data processing, the RMS DS of each measured position was also estimated with a 20 dB threshold from the peak in each PDP and classified based on the relative angular direction between the Tx and Rx antennas into LoS and OLoS. The results indicate that the OLoS case has higher RMS DS values than the LoS case. In both LoS and OLoS scenarios, the cross-polarized link has a greater delay spread value than the co-polarized link. This is due to the antenna beams being misaligned or the LoS component being obstructed, as well as the existence of several MPCs. The CDFs were fitted with a Gaussian normal distribution $N(\mu, \sigma)$ to characterize the delay spread. For each measured environment, Table 5 provides a summary of the 10%, 50%, and 90% CDF values, as well as the estimated parameter of the distribution (σ).

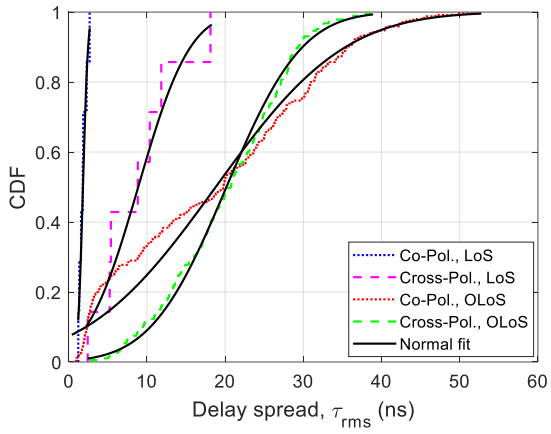

Fig. 13: CDF of RMS DS for an office room environment.

Table 5: RMS DS statistics in (ns) for the different measured environment.

Type of Env.	CDF of RMS DS Statistics	LoS scenario		OLoS scenario	
		Co-Polar	Cross-Polar	Co-Polar	Cross-Polar
Office room	10 %	1.22	2.42	2.33	9.47
	50 %	1.67	7.11	19.78	20.52
	90 %	2.41	13.72	35.51	29.22
	σ	0.52	5.22	12.95	7.59
Meeting room	10 %	1.41	2.09	1.52	2.94
	50 %	1.53	2.42	8.14	7.29
	90 %	2.34	3.57	17.76	12.16
	σ	0.54	0.74	6.59	3.45
Computer lab.	10 %	0.66	1.42	2.04	3.92
	50 %	1.53	2.57	10.07	6.91
	90 %	2.01	4.01	20.35	14.73
	σ	0.57	1.28	7.08	4.47

Based on the ITU model in Recommendation ITU-R P.1238, the delay spread was modeled as a function of the surface area of the observed environment. For different polarization links, a novel model of RMS DS values as a function of room size was generated for different possible antenna alignments. The measured RMS DS values (in $\log_{10}$-scale) versus different room sizes are displayed in Fig. 14. The solid lines in this figure indicate the linear fits of the measured RMS DS to the ITU model in different environments. The predicted model parameters based on the linear fit of the delay spread over different surface areas are shown in Table 6. The obtained results for both polarization links at different possible antenna orientations show that the model has a positive slope (α), indicating that RMS DS increases as the distance between the Tx-Rx antennas increases due to an increase in the attenuation of the LoS component with distance, while the scattered components increase relatively. Furthermore, the results demonstrate that as the size of the room increases, the delay spread values tend to increase. This table also reveals that the Root Mean Square Error (RMSE) varied in a small range of 1.568 – 4.164 for both polarization links, which indicates a better fit to the measured RMS delay spread.

Table 6: ITU model parameters for the RMS DS as a function of the room size.

Beam direction	Polarization links	59.6 – 56.6 GHz		
		α	β	RMSE
LoS	Co-polar	0.488	1.074	1.568
	Cross-polar	16.41	-25.55	2.240
OLoS	Co-polar	11.14	-11.94	4.164
	Cross-polar	16.95	-22.47	2.274

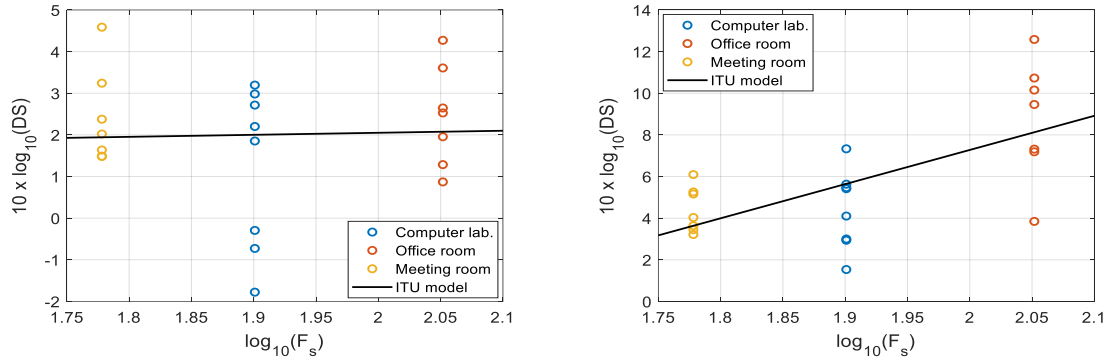

(a) LoS, Co-Polar. (b) LoS, Cross-Polar.

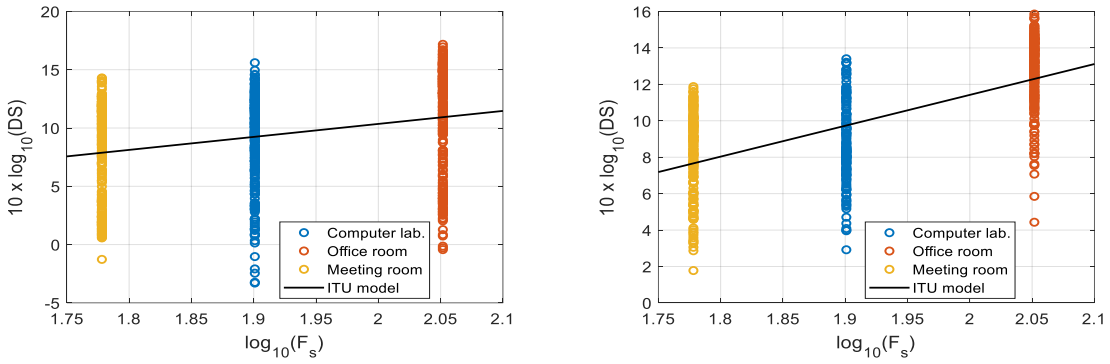

(c) OLoS, Co-Polar. (d) OLoS, Cross-Polar.

Fig. 14: RMS DS values vs. the size of the environment (logarithmic units) based on the ITU model.

- **Angular Spread (AS)**

The azimuth angular spread was estimated from the measured PAP, where the PAP is the received power at each azimuth angle. Fig. 15 shows an example of the computed PAP in one location for the co- and cross-polarized links in the office room environment. The CDFs of the computed AS values for the co-polarized link and the cross-polarized in the office room are shown in Fig. 16 which shows that the co-polarized link exhibits lower average AS values compared with cross-polarized link. This might be due to the power distribution of the cross-polarized link being more uniform across the AoA. The 10%, 50%, and 90% CDF values of the AS and the corresponding standard deviation ($\sigma_{\emptyset_{AS}}$) are given in Table 7. As can be seen, a maximum difference is ~ 31^{o} between the two-polarized links across the measured environments for the 50% of the CDF values. The results also indicate that the meeting room, which is the smallest in size, had a lower AS value, which could be due to a smaller number of reflectors and scatterers.

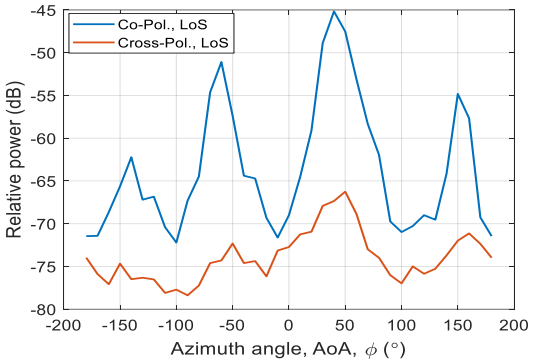

Fig. 15: Power angle profile in an office room environment.

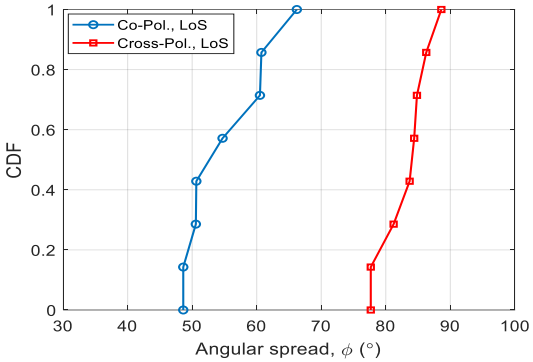

Fig. 16: CDF of AS for an office room environment.

Table 7: AS statistics in degrees (°) for the different measured environment.

Type of Env.	**CDF of RMS DS Statistics**	**LoS scenario**	
		Co-Polar	**Cross-Polar**
Office room	10 %	48.62	77.67
	50 %	52.67	84.05
	90 %	62.37	86.97
	σ	6.60	3.53
Meeting room	10 %	42.34	38.30
	50 %	51.81	54.47
	90 %	61.15	61.68
	σ	7.01	8.79
Computer lab.	10 %	39.98	46.54
	50 %	45.91	54.33
	90 %	58.02	80.39
	σ	13.74	14.51

The AS was estimated as a function of the surface area of the observed environment, according to equation (3) in Recommendation ITU-R P.1238. For different polarization links, a novel model of angular spread values as a function of room size was generated. Fig. 17 shows the measured AS values (in $\log_{10}$-scale) for the co-polarized and cross-polarized links in the 60 GHz band versus different environment sizes. The predicted angular spread as well as the linear fits to the ITU model are also shown in the figure. Table 8 displays the estimated model parameters based on the linear fit of the angular spread values over different room sizes. The obtained results for both polarization links reveal that the linear fit has a positive slope (α) indicating that the AS increases as the distance between the Tx-Rx antennas increases. Furthermore, the results illustrate that angular spread tends to be larger as the size of the room increases, which could be attributed to the large number of reflectors and scatterers within the room. Table 7 also shows that the RMSE is lower than 1 for both polarization links, which indicates a better fit to the measured angular spread values.

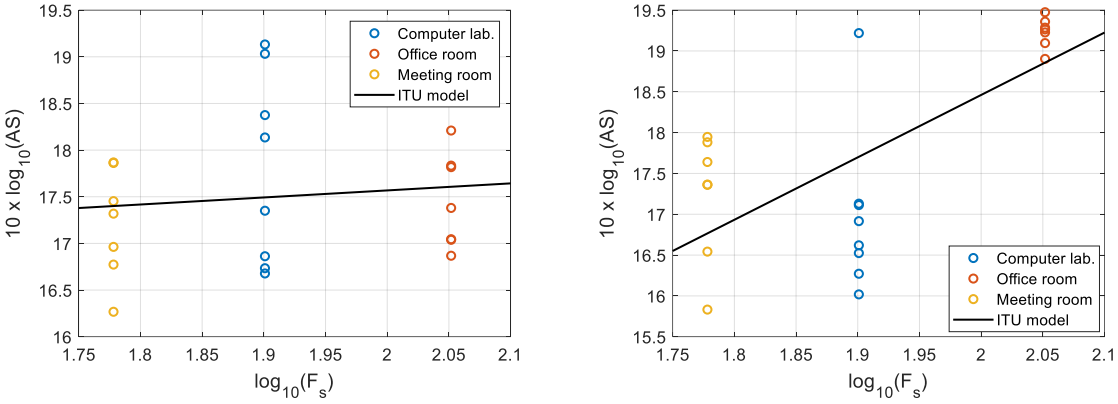

(a) LoS, Co-Polar. (b) LoS, Cross-Polar.

Fig. 17: AS values vs. the size of the environment (logarithmic units) based on the ITU model.

Table 8: ITU model parameters for the AS as a function of the room size.

Beam direction	**Polarization links**	**59.6 – 56.6 GHz**		
		α	**β**	**RMSE**
LoS	Co-polar	0.755	16.06	0.772
	Cross-polar	7.643	3.175	0.929

5. Human Blockage Measurements

5.1 Measurements Methodology

The multiband FMCW channel sounder was also used to measure the shadowing attenuation by one to two persons in an indoor environment. The human blockage measurements were performed in a practical usage environment (computer clusters) which is furnished with multiple chairs, desks, tables, and several computers. The measurements were conducted with different Tx and Rx configurations: antenna heights (Tx = 2.3 m, 1.4 m with Rx = 1.4 m), at 62 GHz. Directional standard horn antennas with a typical gain of 20 dBi (~18° half power beamwidth (HPBW)) were employed at the Tx and Rx. Initially, the received power was measured without blockage and represented by p_o. The received power was then measured by having one or two people walk along or across the Tx-Rx connecting link and represented by p_{sh}. As a result, the loss due to human obstruction is computed as $L\ (dB) = p_o - p_{sh}$. Fig. 18 shows pictures of the human blockage measurement scenarios. The channel sounder set-up parameters for the measurements are summarized in Table 9. The measured scenarios include three schemes when the Tx and Rx antennas face each other and are separated with 15 m:

- One person of ~1.85 m height, ~0.45 m shoulder width, and ~0.25 m depth walks along the Tx-Rx connecting link (LoS path) starting from 2 m to 13 m with a 0.5 m step, as shown in Fig. 19 (a).
- One person of ~1.85 m height, ~0.45 m shoulder width, and ~0.25 m depth walks perpendicular to the LoS path at (3.6 m, 7.5 m, and 11.4 m) from -1 m to 1 m of the Tx-Rx connecting link with a 0.25 m step, as shown in Fig. 19 (b).
- Two persons of ~1.85 m height, ~0.45 m shoulder width, and ~0.25 m depth walk in parallel across the LoS path at (7.5 m and 11.4 m) from -1 m to 1 m of the Tx-Rx connecting link with a 0.25 m step, as shown in Fig. 19 (c).

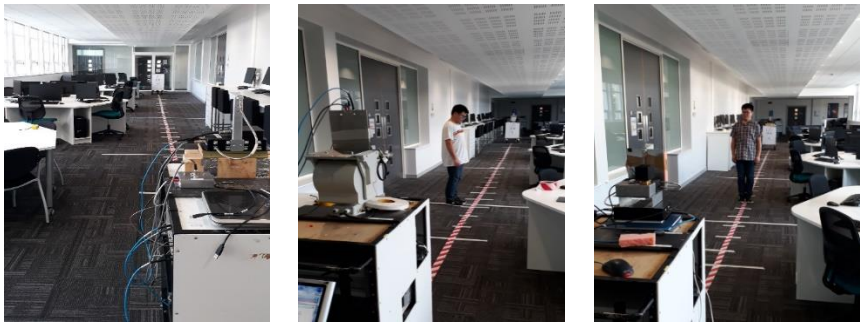

(a) Same Tx-Rx height configuration.

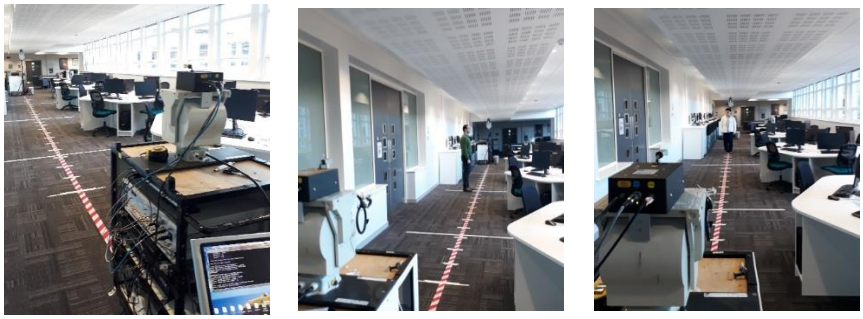

(b) Different Tx-Rx height configuration.

Fig. 18: Photos of the indoor human blockage measurement scenarios.

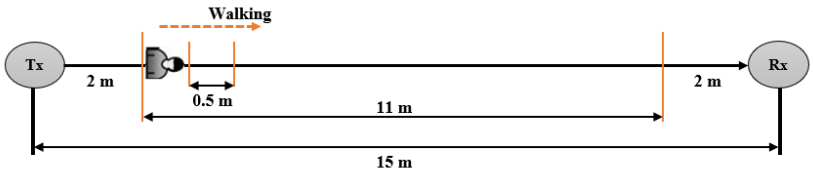

(a) One person walks along the LoS path.

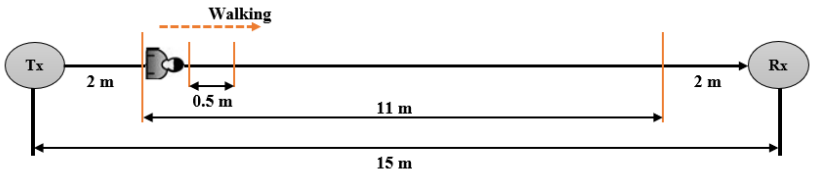

(b) One person crosses the LoS path.

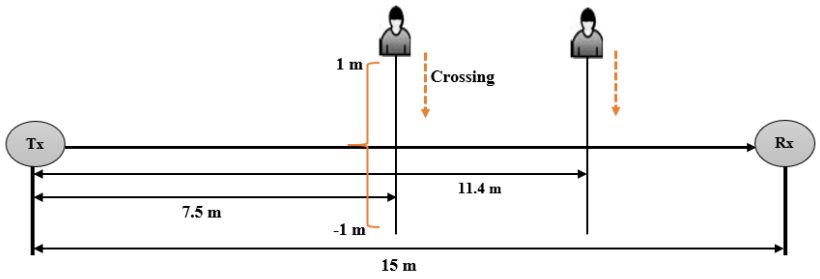

(c) Two persons cross the LoS path.

Fig. 19: Layout of the indoor human blockage measurement scenarios.

Table 9: Channel measurements set-up parameters.

Frequency Range	**59.6 – 65.6 GHz**
RF bandwidth	6 GHz
Analysis bandwidth	2 GHz
Sampling rate	40 MHz
Sweep rate	1.22 kHz
Record duration	1s
Tx Antenna (gain, beam)	20 dBi, Horn (~18^{o})
Rx Antenna (gain, beam)	20 dBi, Horn (~18^{o})
Tx/Rx polarization	Vertical-Vertical (V - V)
Tx antenna height	2.3 m (1.4 m)
Rx antenna height	1.4 m

5.2 Results and Analysis

- **Power Delay Profile (PDP)**

Fig. 20 shows an example of the measured PDPs when a person walked along the Tx-Rx connecting link (LoS path). The profiles were normalized with respect to the strongest received component. The figure indicates that the signal strength varied with respect to the distance between the Tx antenna and the person. The PDPs exhibit some variation when the person moved along the measured path as a result of the person becomes a reflector. The lowest signal levels can be seen when the person is either close to the Tx or Rx antenna, while the strongest signal levels appear when the person is around the middle of the transceiver. Fig. 21 shows an example of normalized PDPs with respect to the maximum received component when a person walked across the Tx-Rx connecting link (LoS path). The figure indicates that as the person standing between the Tx and Rx antenna, the direct path and some of the reflected paths were attenuated and blocked. The shadow regions can be seen as the person heavily attenuated the LoS path, while the reflection regions appear when the person started to walk far from the LoS path.

The impact of the human body on the MPCs at 60 GHz when a person walked along or walked across the LoS path are displayed in Fig. 22 (a) and (b), respectively. In this figure, the obstructed PDPs were compared with the unobstructed PDPs. Fig. 22 (a) displays the effect of the human body on the MPCs when a person walked along the LoS path and standing at (D=3.6 m and D=7.5 m) away from the Tx antenna. As seen from Fig. 22 (a), the direct path and the reflected paths of the obstructed PDPs have lower signal level values compared with the unblocked PDPs. Fig. 22 (b) presents the effect of the human body on the MPCs when a person walked across the LoS path and standing at (D=0 m and D=0.3 m) away from the LoS path. It can be observed that the direct path and the reflected paths when the person was standing at (D=0 m) have the lowest power level values, where the human body is heavily attenuating the LoS path and some of the reflected paths.

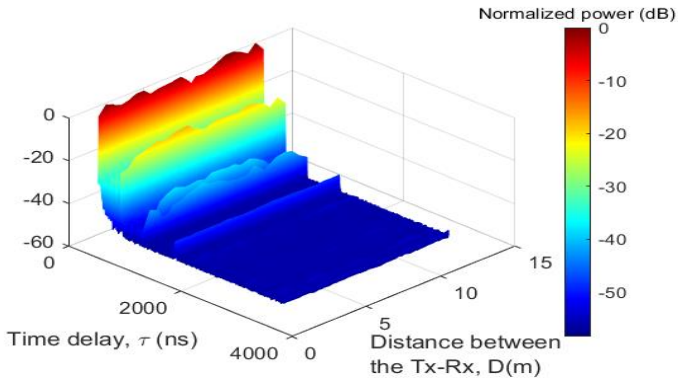

Fig. 20: Examples of measured PDPs with HB walked along the LoS path.

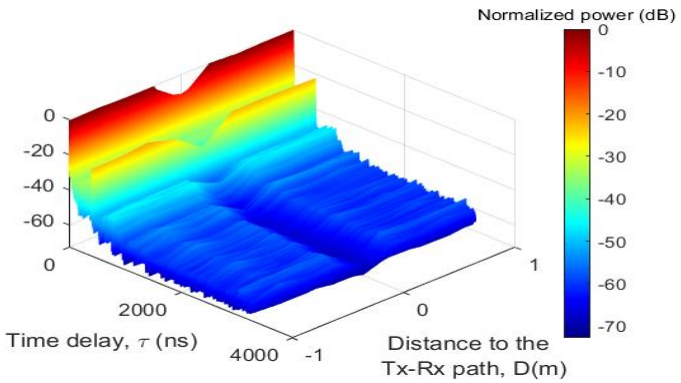

Fig. 21: Examples of measured PDPs with HB walked across the LoS path.

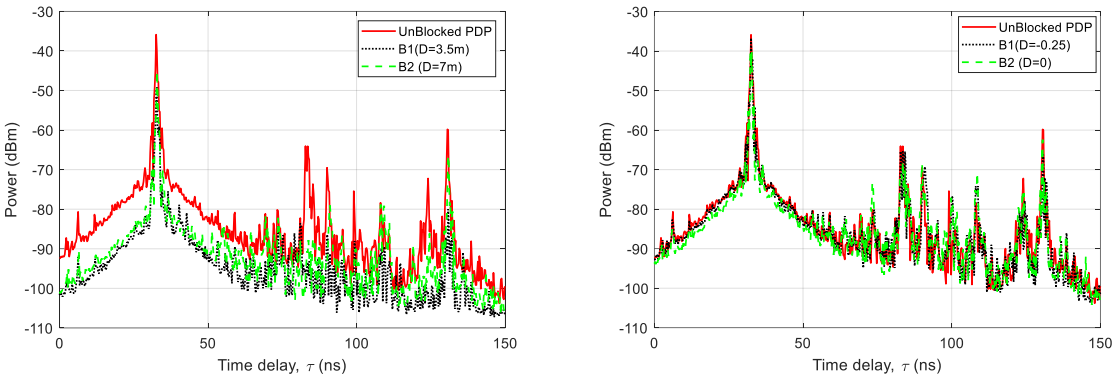

(a) 62 GHz, one person walks along (b) 62 GHz, one person walks across.

Fig. 22: Examples of single PDP with effect of HB on the MPCs.

- **One person moves along the Tx-Rx connecting link (LoS path)**

Fig. 23 (a) presents the measurement and modelling of the HB attenuations when a person moves along the LoS path with the same Tx-Rx antenna height configurations. It can be clearly seen from this figure that the largest measured attenuations occurred as the person was either near the Tx or Rx antenna. The measured HB attenuations at the 60 GHz bands agree well with the METIS KED, Kirchhoff KED, and GTD models, but at some points, the measured results are higher than the modelling results due to the diffraction waves arriving at the Rx, which include the diffraction signal from the human body effects. The losses caused by the human body for the same Tx-Rx antennas height over this band varied in the range between (~ -10 dB) and (~ -17 dB).
Fig. 23 (b) presents the measurement and modelling of the HB attenuation when a person moves along the LoS path with different Tx-Rx antenna height configurations. It can be clearly seen from this figure that the measured attenuations tend to be higher as the person moved away from the Tx side. This figure indicates that the human body becomes a scatterer as the person moves along the LoS path and the largest losses occur when the person was close to the Rx antenna. The maximum losses caused by the human body for the different Tx-Rx antenna heights is around (~ -7 dB). The measurements with different antenna height configurations are fitted well with the exponential distribution.

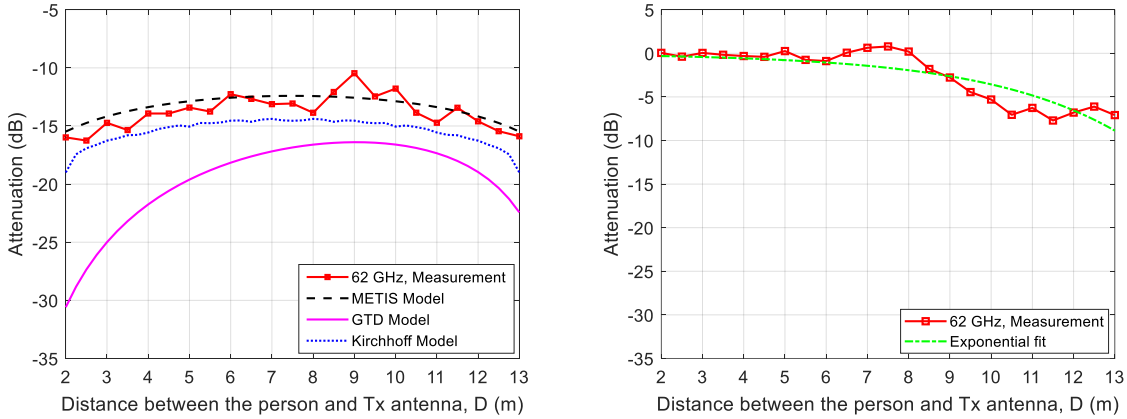

(a) Same Tx-Rx height. (b) Different Tx-Rx antenna height.

Fig. 23: Measurement and modelling HBS attenuations with a person walks along the LoS path

- **One person moves along the Tx-Rx connecting link (LoS path)**

Fig. 24 displays the measurements and modelling of the HB attenuations with a person crossing the Tx-Rx connecting link (LoS path) in one position. As seen from Fig. 24, both the METIS KED and Kirchhoff KED models are fitted well with the measurement data, while the GTD model overestimated the losses across the measured band. The measurements of HB attenuation with the same Tx-Rx antenna height configurations when a person walked across the LoS path at three different positions are presented in Fig. 25 (a). It can be seen from the figure that the deep fading occurred as a person obstructed the LoS path and the highest loss is either crossing near the Tx or Rx antenna. The HB measurements with different Tx-Rx antenna height configurations are presented in Fig. 25 (b). In this figure, deep fading and the highest attenuation occurred when a person crossed the LoS path close to the Rx antenna, where the person becomes a scatterer when crossing the LoS path at positions that are far away from the Rx antenna.

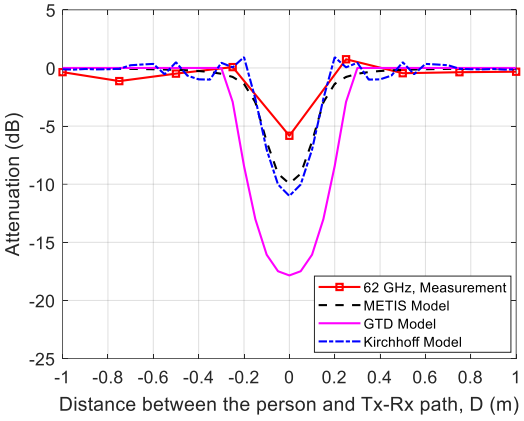

Fig. 24: Measurement and modelling HBS attenuations with a person crossing the LoS path at the same Tx-Rx antenna height.

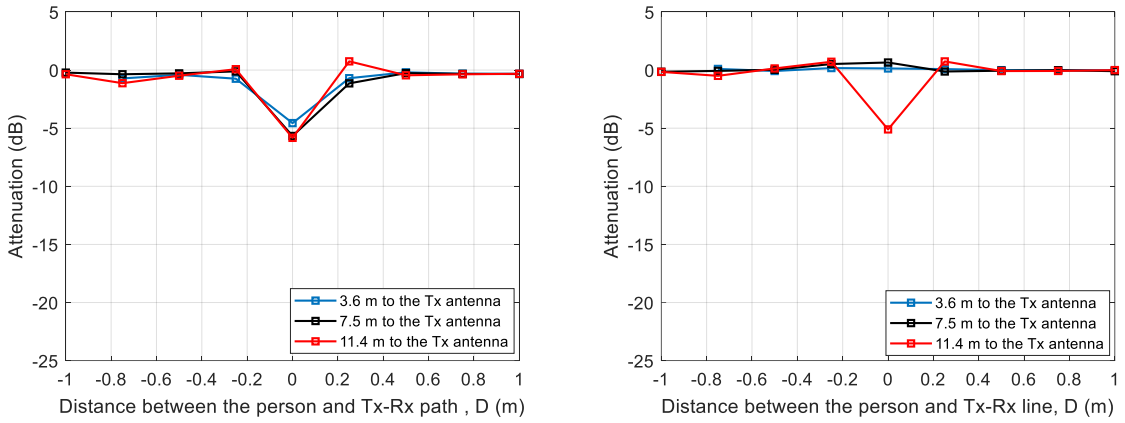

(a) Same Tx-Rx height. (b) Different Tx-Rx height.

Fig. 25: Examples of HBS attenuations measurement with a person crossing the LoS path.

- **Two person moves along the Tx-Rx connecting link (LoS path)**

Fig. 26 displays the measurement and modelling of HB attenuation over multiple bands with two persons moving across the LoS path for the same Tx-Rx antenna height. The METIS KED model was employed to model the impact of the HBS attenuation. The measured HBS attenuation matches well

with the model. It is noticeable that the losses are greater than 0 dB at some point as a result of the human body acting as a scatterer when the LoS path is unobstructed. Furthermore, the results illustrate that not much difference in the attenuation either with one or two persons walking across the LoS path.

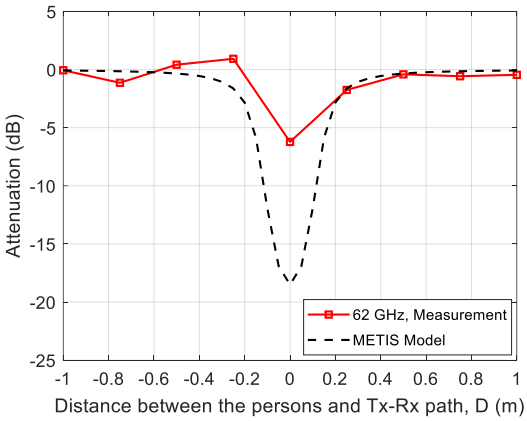

Fig. 26: Measurements and modelling HBS attenuation with two persons walk across the LoS path at the same Tx-Rx antenna height.

6. Measurement based simulations

6.1 Measurement methodology

For further research one of the measured scenarios was simulated in the ray tracing (RT) simulator developed at UPV [17]. The measurements were described in [18]. The environment, which is the meeting room at Durham University, is presented in Fig. 10(a). However, the measurement setup was different than described in sections 4 and 5. The measurements were also conducted using Durham University FMCW channel sounder [8]. The measured environment is set up with multiple chairs, and a table. The measurements were performed with a 6 GHz bandwidth in the 60 GHz ISM band with a waveform repetition frequency of 1.22 kHz. A horn antenna was used at the Tx side, while an omni-directional antenna was used at the Rx. The measurements were conducted in a LoS scenario with the Tx location fixed at the corner of the room while the Rx was moved onto 16 predefined locations within the scenario as shown in Fig. 27. The arrow at the Tx position represents the main beam's direction at a rotation angle of 0°. The Tx antenna height was set at 2.8 m which is close to the typical height of an access point, while the Rx antenna was set at 1 m for typical equipment installed on the table. To investigate the wideband channel in the angular domain, a CCTV rotator is used to steer the directional antenna in steps of 15° to cover the full rotation in the azimuth plane. Therefore, 24 data files were recorded at each location, corresponding to the full 360° azimuthal coverage. At each angular rotation, the data were recorded for one second with a 40 MHz sampling rate ADC. Table 10 gives a summary of the channel measurement set-up parameters for the measured environment.

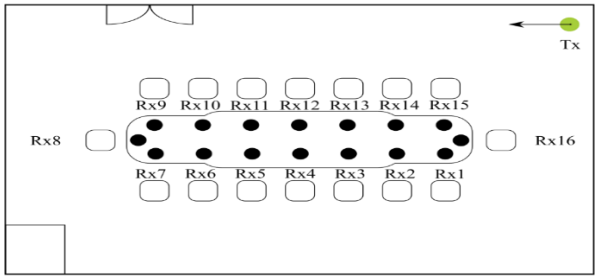

Fig. 27: Layout of the meeting room.

Table 10: Channel measurements set-up parameters.

Frequency Range	**59.6 – 65.6 GHz**
RF bandwidth	6 GHz
Analysis bandwidth	2 GHz
Sampling rate	40 MHz
Sweep rate	1.22 kHz
Record duration	2s
Tx Antenna (gain, beam)	20 dBi, Horn (~18^o)
Rx Antenna	Omni-directional
Tx/Rx polarization	Vertical-Vertical (V - V)
Tx antenna height	2.8 m
Rx antenna height	1 m

6.2 Simulation evaluation

The meeting room was recreated in the RT simulator. The top view with chairs, table, whiteboards on the wall, door, glass, and plasterboard walls are visible from the top view in Fig. 28. Based on the dimension measurements the exact size of the furniture and surroundings were introduced to the RT simulator. Also, the information about materials from which the furniture was built, i.e. wood, plastic, was introduced for each item inside the room. Positions of the Rx were also measured, thus the chairs in the simulated environment were settled exactly in front of each Rx position and turned to face the table.

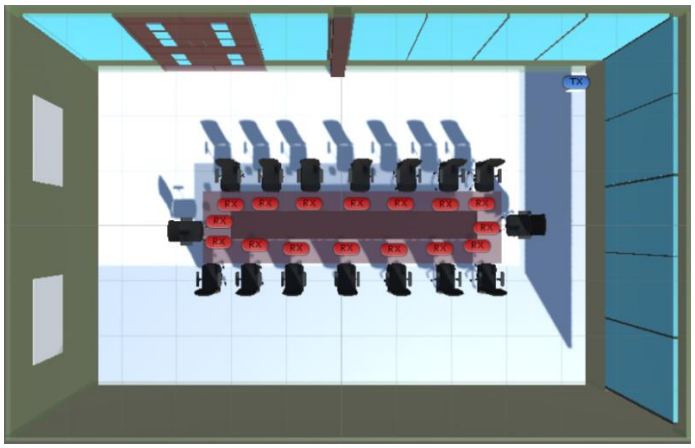

Fig. 28: The meeting room created in the RT simulator.

Fig. 29 shows the result of the comparison of measured and simulated data after adjusting the environment based on the photographs and a few rounds of simulations. Fig. 29 (a) shows power received at each of the 16 Rx positions when the Tx antenna was turned in the Rx antenna's direction. For positions 1-9 the environment is well adjusted. The larger differences are for positions 10-16, where the impact of chairs' height and positions may be crucial. It is visible especially for position 15 where it is a great probability that the LoS was blocked. Fig. 29 (b) shows the RMS DS. There are two Rx positions for which RMS DS was much higher than for others. We conclude that for the Rx position 10 there was an additional strong reflection that was coming from an object unidentified in the environment, probably the trolley with the measuring equipment. For Rx position 15 we assumed NLoS condition.

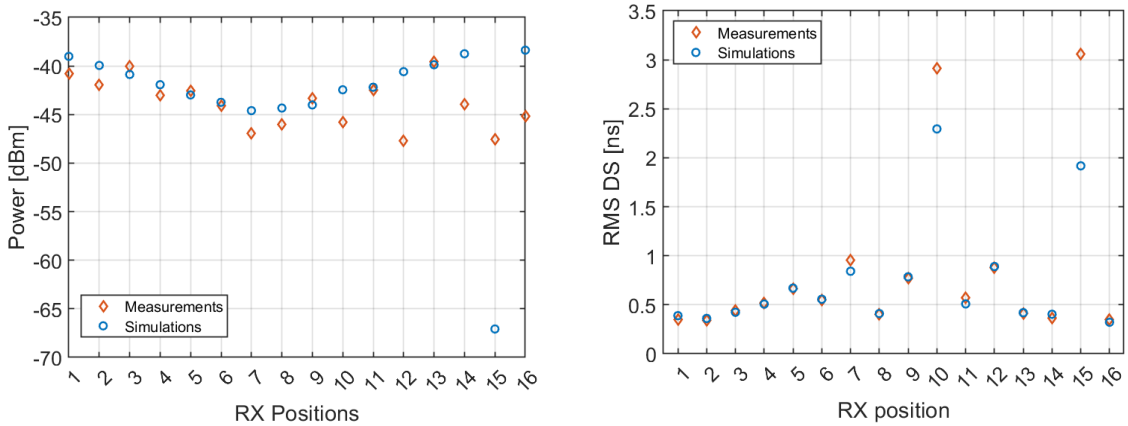

(a) power received in LoS direction (b) RMS DS

Fig. 29: Measured and simulated values of received power and RMS DS for each of 16 Rx positions.

6.3 Impact of the room size

It is not easy to compare the measured values of the channel parameters in different environments. Even if the dimensions are the same the furniture setup or used materials might be different. In the simulations, it is possible to modify the room dimensions and evaluate the changes that are introduced because of that. To see the impact of the room size three different rooms were simulated. Their dimensions are listed in Table 11.

Table 11: Simulated rooms dimensions.

	Length [m]	Width [m]	Height [m]
Room SIM	8.8	7.9	2.9
Room I	20.2	13.1	6
Room II	41	26.6	9

In the scenario, when the dimensions of the room change the position of the Tx antenna changes as well. It is always in the corner to simulate the real scenario, where the antenna is placed on the wall.

Fig. 30 shows the received power and RMS DS for all three rooms listed in Table 11. In Fig. 30 (a) it is shown that for larger rooms, thus the larger distance between Tx and Rx antenna, the received power is decreasing. We can also observe that the object that caused a signal blockage in Rx position 15 no longer impacts the received power. However, in Room II, there is a new object that causes the drop in the received signal in Rx position 2. In Fig. 30 (b) we can observe that the maximum value of RMS DS is larger for larger rooms, but it is always below 3.5 ns. The expected result is that for larger rooms there are more Rx positions in which the RMS DS value is closer to a maximum calculated value.

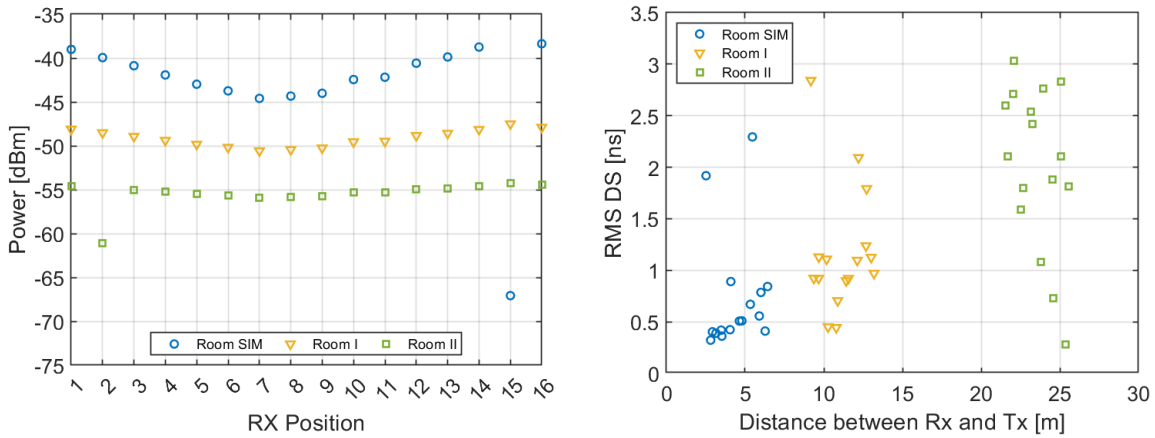

Fig. 30: Values of received power and RMS DS in three simulated rooms.

6.4 Environment simulation guideline

To make the simulation as accurate as possible the environment has to be mapped with great precision. In the case described in this section, the measurements and the simulations were made by separate teams, thus the group who made simulations have never been in the measured room. In spite of that, it should be possible to recreate the environment with the information provided together with the obtained data. We want to share a few thoughts about recording the measurements for further processing in simulations.

- Check the dimensions of the room precisely (height, width, and depth, if possible, in more than one point).
- Check the materials of the walls, floor, and ceiling, and everything that lays or hangs on them.
- Check the dimension, positions, material and furniture inside the room.
- Make a lot of photos. First of the room without the measurement equipment. It may be helpful to make a 360° video.
- Make photos during the measurements. The position of the measurement equipment is also very important.
- Check the position and height of the Tx and Rx antennas more than one time.
- Check the position and height of the furniture more than one time, especially if there are chairs or other items that can be easily moved.
- If there is an additional equipment that is moved when the measurements are made make sure to save the information about it.
- The exact height of the furniture is very important due to diffraction.

7. Conclusion

In this document, indoor SISO and SIMO channel measurements were conducted at Durham University in the 60 GHz ISM band in multi-scenarios using a custom-designed channel sounder. The present measurements aim to characterize the spatial and temporal variation of the channel. It was observed that the OLoS scenario has higher RMSDS values compared with the LoS scenario when the antennas become misaligned due to the large number of obstructions and multipath components. Moreover, the results observed that the co-polarized links exhibited lower RMS DS and AS values compared with the cross-polarized links. The AS values emphasize the fact that indoor environments have larger angular spread values than outdoor environments due to the larger number of multipath components within indoor scenarios. The relationship between the delay spread and the angular spread with room size agrees well with the ITU model and is found to be linear with a positive slope.

Human body attenuation in the 60 GHz band was also investigated by real-time measurements and modelling. The blockage effects of the human body have been measured and analysed for three different cases. The attenuation shows a variation when a person walks along the LoS path, while deep fading occurs as a person walks across the LoS path. Blockage models such as the GTD model, Kirchhoff model, and METIS model have been applied to model human shadowing attenuation effects. The presented blockage modelling results fit well with the measurement data.

The simulations performed based on the measurements show how important it is to properly describe the environment and the measurement procedure. It is due to the great impact that all objects have on the transmission in the 60 GHz band. Slightly different position or the lack of some object in the surroundings can change the results significantly. The impact of the far away objects will be smaller in larger environments. Along with the distance between the Tx and Rx antennas the received power will be decreasing, and the RMS DS will be increasing. However, in the LoS conditions the increase of RMS DS in the investigated environments was small.

8. References

[1] X. Wu et al., "60-GHz Millimeter-Wave Channel Measurements and Modeling for Indoor Office Environments," in IEEE Transactions on Antennas and Propagation, vol. 65, no. 4, pp. 1912-1924, April 2017.

[2] G. R. Maccartney, T. S. Rappaport, S. Sun and S. Deng, "Indoor Office Wideband Millimeter-Wave Propagation Measurements and Channel Models at 28 and 73 GHz for Ultra-Dense 5G Wireless Networks," in IEEE Access, vol. 3 pp. 2388-2424, 2015.

[3] J. Huang, C.-X. Wang, R. Feng, J. Sun, W. Zhang, and Y. Yang, "Multi-frequency mmWave massive MIMO channel measurements and characterization for 5G wireless communication systems," IEEE J. Sel. Areas Commun., vol. 35, no. 6, June 2017, in press.

[4] J. Zhu, H. Wang and W. Hong, "Large-scale fading characteristics of indoor channel at 45-GHz band," IEEE Antennas and Wireless Propagation Letters, 2015, 14, pp. 735-738.

[5] K. Haneda, J. Järveläinen, A. Karttunen, M. Kyrö and J. Putkonen, "Indoor short-range radio propagation measurements at 60 and 70 GHz," The 8th European Conference on Antennas and Propagation (EuCAP 2014), The Hague, 2014, pp. 634-638.

[6] Hao Xu, Kukshya, V., Rappaport, T., "Spatial and temporal characteristics of 60-GHz indoor channels," IEEE Journal on Selected Areas in Communications, 2002, 20, (3), pp. 620-630.

[7] Bamba, A., Mani, F., D'Errico, R., "E-band millimeter wave indoor channel characterization," IEEE 27th Annual Int. Symposium on Personal Indoor and Mobile Radio Communications (PIMRC), Valencia, Spain, September 2016, pp. 1-6.

[8] S. Salous, S. M. Feeney, X. Raimundo and A. A. Cheema, "Wideband MIMO Channel Sounder for Radio Measurements in the 60 GHz Band," in IEEE Transactions on Wireless Communications, vol. 15, no. 4, pp. 2825-2832, April 2016.

[9] X. Raimundo, S. Salous and A. Cheema, "Indoor dual polarised radio channel characterisation in the 54 and 70 GHz bands," in IET Microwaves, Antennas & Propagation, vol. 12, no. 8, pp. 1287-1292, 4 7 2018.

[10] Smulders, P. F. (2009). Statistical characterization of 60-GHz indoor radio channels. IEEE Transactions on Antennas and Propagation, 57(10), 2820-2829.

[11] Chen, Xubin, Lei Tian, Pan Tang, and Jianhua Zhang. "Modelling of human body shadowing based on 28 ghz indoor measurement results." In 2016 IEEE 84th Vehicular Technology Conference (VTC-Fall), pp. 1-5. IEEE, 2016.

[12] Ghaddar, M., L. Talbi, and T. A. Denidni. "Human body modelling for prediction of effect of people on indoor propagation channel." Electronics letters 40, no. 25 (2004): 1592-1594.

[13] Gustafson, Carl, and Fredrik Tufvesson. "Characterization of 60 GHz shadowing by human bodies and simple phantoms." In 2012 6th European Conference on Antennas and Propagation (EUCAP), pp. 473-477. IEEE, 2012.

[14] G. R. MacCartney, Jr., S. Deng, S. Sun, and T. S. Rappaport, "Millimeterwave human blockage at 73 GHz with a simple double knife-edge diffraction model and extension for directional antennas," in Proc. IEEE VTC'16-Fall, Montral, Canada, Sept. 2016.

[15] Qi, Wenzhe, Jie Huang, Jian Sun, Yi Tan, Cheng-Xiang Wang, and Xiaohu Ge. "Measurements and modeling of human blockage effects for multiple millimeter Wave bands."

[16] Bamba, A., Mani, F., D'Errico, R., "E-band millimeter wave indoor channel characterization," IEEE 27th Annual Int. Symposium on Personal Indoor and Mobile Radio Communications (PIMRC), Valencia, Spain, September 2016, pp. 1-6.

[17] S. Inca, D. Prado, D. Martín-Sacristán, and J. F. Monserrat, "Channel modelling based on game engines light physics for mmw in indoor scenarios," in 2020 14th European Conference on Antennas and Propagation (EuCAP), pp. 1–5, IEEE, 2020.

[18] A. Al-jzari, J. Towers, and S. Salous, "Characterization of indoor environment in the 60 GHz band," in 2020 XXXIIIrd General Assembly and Scientific Symposium of the International Union of Radio Science, pp. 1–4, IEEE.